

2010

Vortex-assisted DNA delivery

Jun Wang

Purdue University - Main Campus

Yihong Zhan

Purdue University - Main Campus, yzhan@purdue.edu

Victor M. Ugaz

Texas A&M University

Chang Lu

Purdue University - Main Campus

Follow this and additional works at: <http://docs.lib.purdue.edu/nanopub>



Part of the [Nanoscience and Nanotechnology Commons](#)

Wang, Jun; Zhan, Yihong; Ugaz, Victor M.; and Lu, Chang, "Vortex-assisted DNA delivery" (2010). *Birck and NCN Publications*. Paper 617.

<http://docs.lib.purdue.edu/nanopub/617>

This document has been made available through Purdue e-Pubs, a service of the Purdue University Libraries. Please contact epubs@purdue.edu for additional information.

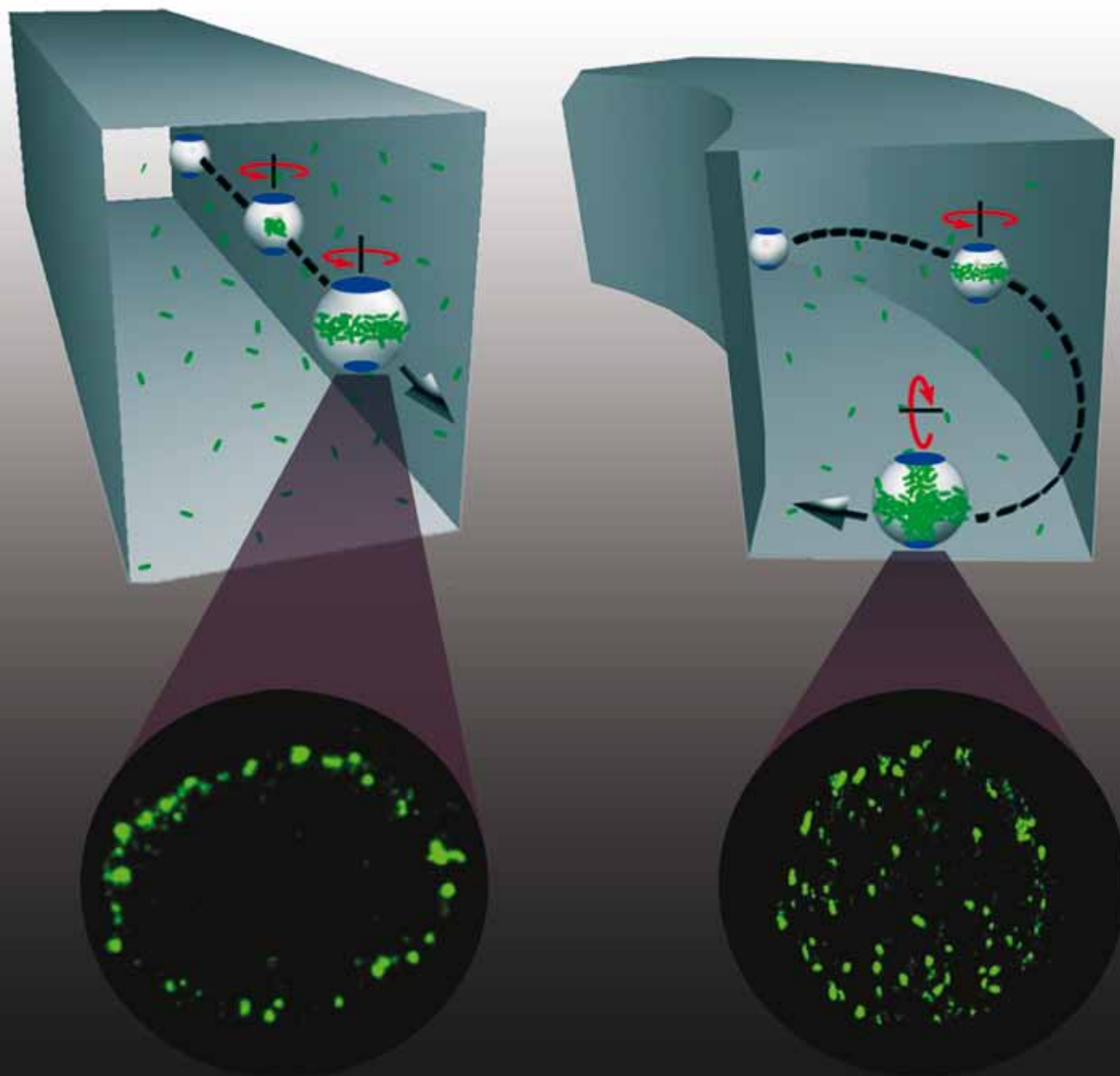
Lab on a Chip

Micro- & nano- fluidic research for chemistry, physics, biology, & bioengineering

www.rsc.org/loc

Volume 10 | Number 16 | 21 August 2010 | Pages 2005–2176

Downloaded by Purdue University on 21 October 2010
Published on 21 June 2010 on http://pubs.rsc.org | doi:10.1039/C004472E



ISSN 1473-0197

RSC Publishing

Lu
Vortex-assisted DNA delivery
Beebe
Cell programmable assay chips

Levchenko
Lab-on-a-chip for stem cell biology
Lu
Extraction of subcellular proteins

Vortex-assisted DNA delivery†

Jun Wang,^a Yihong Zhan,^a Victor M. Ugaz^b and Chang Lu^{*c}

Received 18th March 2010, Accepted 4th June 2010

DOI: 10.1039/c004472e

Electroporation is one of the most widely used methods to deliver exogenous DNA payloads into cells, but a major limitation is that only a small fraction of the total membrane surface is permeabilized. Here we show how this barrier can be easily overcome by harnessing hydrodynamic effects associated with Dean flows that occur along curved paths. Under these conditions, cells are subjected to a combination of transverse vortex motion and rotation that enables the entire membrane surface to become uniformly permeabilized. Greatly improved transfection efficiencies are achievable with only a simple modification to the design of existing continuous flow electroporation systems.

Introduction

Delivery of exogenous DNA payloads into cells (*i.e.* gene transfer or transfection) is a critical step in cell-based therapeutics, tissue engineering, and fundamental molecular and cell biology. This process is often accomplished by electroporation, a method that involves applying electrical pulses to open transient nanoscale pores in the cell membrane that permit entry of impermeant DNA. Electroporation methods are advantageous due to their simplicity and capacity for operation in a high-throughput continuous flow manner¹ and in microscale devices,^{2–6} but they are also extremely inefficient. These limitations arise as a consequence of the fundamental interactions between the cells and the applied electric field whereby favorable permeabilization conditions (*i.e.*, transmembrane potential exceeding a critical threshold value of ~ 0.25 – 1 V) can only be achieved over a very small fraction of the total membrane surface. This can be seen by considering the transmembrane potential distribution over a spherically shaped cell ($\Delta\psi_E = 0.75 \frac{g(\lambda)aE}{\cos\theta}$, where $g(\lambda)$ is a complex function of the membrane and buffer conductivities, a is the diameter of the cell, E is the field strength and θ is the angle between the normal to the membrane surface and the field direction⁷) which shows that DNA transfer is favored only near the poles (*i.e.*, $\theta \rightarrow 0$) where the surface normal is closely aligned with the field direction, as has been observed experimentally.^{8,9} The size of this zone cannot be expanded by increasing the electric field because the cells will become damaged and experience dramatically reduced viability. Applying periodic electric pulses of different polarities and directions was shown to improve gene transfer.¹⁰ However the instrument complexity required to employ this approach is relatively high, with limited feasibility for scale-up to processing large numbers of cells.

In this report we introduce a new approach to overcome these limitations by harnessing hydrodynamic effects that arise in fluidic networks incorporating curved flow paths. Under appropriate conditions, the curvature-induced inertial force acting along the channel's radius of curvature becomes strong enough to establish a transverse vortex flow superimposed over the fluid's axially directed pressure driven motion. When a cell laden suspension encounters such a flow field, the cells are simultaneously subjected to a complex combination of transverse advection and rotation. In this way, a much larger fraction of the total cell surface is able to experience alignment with the electric field and become permeabilized, so that it can be accessed by exogenous DNA. We show that electroporation in this curved spiral-shaped channel design yields a two-fold increase in transfection efficiency compared to a straight microchannel.

Materials and methods

Materials

Fluorescent polystyrene beads with diameter $9.9 \pm 0.05 \mu\text{m}$ (s.d.) were purchased from Duke Scientific. The density of beads is 1.05 g/ml according to the protocol. Before experiment, the beads were diluted in phosphate buffered saline (PBS) at a concentration of $1.9 \times 10^6/\text{ml}$. The 4.7 Kb plasmid vector pEGFP-C1 (Clontech) coding green fluorescent protein (GFP) was propagated in *Escherichia coli* and extracted in Tris-EDTA buffer with QIAfilter Plasmid Giga kit (Qiagen). The plasmid was stained with green fluorescent DNA dye YOYO-1 (Invitrogen) with a molecular ratio of 1 dye per 5 bp when fluorescent labeling was necessary. Chinese hamster ovary (CHO-K1) cells were grown using protocols provided by ATCC. To observe flowing cells in microfluidic channels, CHO cells were stained by $5 \mu\text{M}$ nucleic acid dye SYTO 16 (Invitrogen) for 5 min followed by washing.

Microchip fabrication

Microfluidic devices were fabricated on polydimethylsiloxane (PDMS, General Electric Silicones RTV 615) using standard soft lithography as we demonstrated previously.¹¹

^aBirck Nanotechnology Center, Purdue University, West Lafayette, Indiana, 47907, USA

^bArtie McFerrin Department of Chemical Engineering, Texas A&M University, College Station, Texas, 77843, USA

^cDepartment of Chemical Engineering, Virginia Tech, Blacksburg, Virginia, 24061, USA. E-mail: changlu@vt.edu

† Electronic supplementary information (ESI) available: Supplementary Fig. S1 and S2; Movies 1–3. See DOI: 10.1039/c004472e

Fluorescence microscopy

To show the flow pattern of cells and particles in microfluidic channels, CHO cells were labeled with SYTO 16 and 100~200 consecutive fluorescence images were taken with 40 ms exposure time for each of them and superimposed for image analysis. The delivery of YOYO-1 labeled pEGFP-C1 into cells was observed using a confocal fluorescence microscope (LSM 510, Carl Zeiss) with a 63X, 1.4 NA oil-immersion objective. In order to observe the delivery of the plasmid under confocal microscope, 500 $\mu\text{g}/\text{ml}$ fluorescent plasmid was mixed with CHO cells in the electroporation experiment. These processed cells were moved to a centrifuge tube immediately after electroporation and washed twice to remove nonspecifically adsorbed DNA molecules from the cell surface before imaging.

Microchip operation

The microfluidic electroporation device was mounted on an inverted fluorescence microscope (IX-71, Olympus) (as shown in ESI Fig. S1†). The inlet of the channel was connected to a syringe pump (PHD infusion pump, Harvard Apparatus) by plastic tubing through which cells or beads were pumped into the microfluidic devices at a constant flow rate. A high voltage power supply (PS350, Stanford Research Systems) was used to generate a constant direct current (DC) voltage between the sample and the outlet reservoirs. Electroporation occurred when cells flowed through the narrow section of the channel where the field intensity was higher than the electroporation threshold.^{1,12}

Transfection

Cells were centrifuged at 260 g for 5 min and resuspended at 2×10^6 cells/mL in the electroporation buffer (8 mM Na_2HPO_4 , 2 mM KH_2PO_4 , and 250 mM sucrose, pH = 7.2) containing 10 $\mu\text{g}/\text{ml}$ plasmid. After electroporation under certain electric parameters in the microfluidic devices, the cells were cultured in DMEM medium for 2 days before quantification of transfection frequency and viability. Transfection efficiency is the percentage of EGFP expressing cells among living cells. The cell viability after electroporation was assessed by staining cells with propidium iodide (PI, Invitrogen) and calculated by dividing the number of viable cells by the total number of cells. All data points were generated by experiments in triplicate and $\sim 5,000$ cells were examined in each trial. Two-tailed student's t test was applied to evaluate the data.

Results

We first examined the effects of hydrodynamics on the migration of cells and particles (including Chinese hamster ovary (CHO) cells with $a \sim 14.6 \pm 2.2$ μm (s.d.) and polystyrene beads with $a \sim 9.9 \pm 0.05$ μm (s.d.)) in microfluidic channels incorporating a central spiral section of reduced cross-section (*i.e.*, the electroporation zone). The migration of cells or beads in the spiral channel is affected by a balance between (1) transverse lift forces that act to stabilize them at distinct equilibrium positions within the microchannel cross section, and (2) a centrifugal Dean force that acts to entrain them in a counter-rotating transverse vortex flow pattern.¹³ The interplay between these effects can be seen in

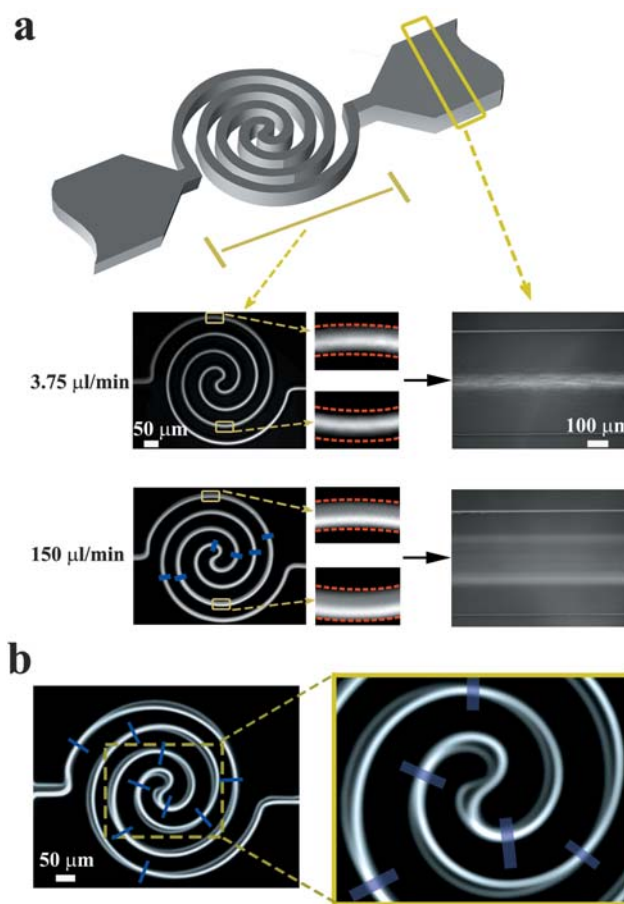


Fig. 1 Particle migration in a flow-through electroporation device with a spiral electroporation section. The device has two wide sections (each is 3 cm long and 500 μm wide) and one narrow section (4.768 mm long and 35 μm wide). The depth of the channel is 75 μm . The narrow section has a spiral shape (with the largest curvature R_{max} of 330 μm and the smallest curvature R_{min} of 30 μm). (a) Overlay fluorescence images of SYTO 16 stained CHO cells flowing in the device at flow rates of 3.75 and 150 $\mu\text{l}/\text{min}$. (b) Overlay fluorescence image of polystyrene beads flowing in the spiral section at 150 $\mu\text{l}/\text{min}$. The blue bars mark the locations where the bead stream shifts across the centerline of the channel.

Fig. 1a, where a suspension of CHO cells is loosely focused at the channel centerline throughout the entire spiral section (height ~ 75 μm , width ~ 35 μm) when the flow rate is low (3.75 $\mu\text{l}/\text{min}$). As the flow rate increases to 75–150 $\mu\text{l}/\text{min}$ the Dean drag begins to dominate and the focused stream of CHO cells becomes displaced, crossing the centerline at multiple locations along the spiral section (Fig. 1a). This transverse motion indicates that the CHO cells are entrained in the Dean vortex flow pattern at high flow rates. Similar transverse advection can be observed more readily when a suspension of the fluorescent polystyrene beads flows through the same spiral-shaped channel at 150 $\mu\text{l}/\text{min}$ (Fig. 1b). As a comparison and control, we also studied migration of the cells and polystyrene beads in a device where the spiral channel is replaced with a straight section of identical length, width and depth. In this geometry, CHO cells gradually focus to the centerline as they travel through the narrow section at the low flow rate of 3.75 $\mu\text{L}/\text{min}$ (Fig. 2). At higher flow rates (37.5–150 $\mu\text{L}/\text{min}$) the CHO cells become focused into two streams

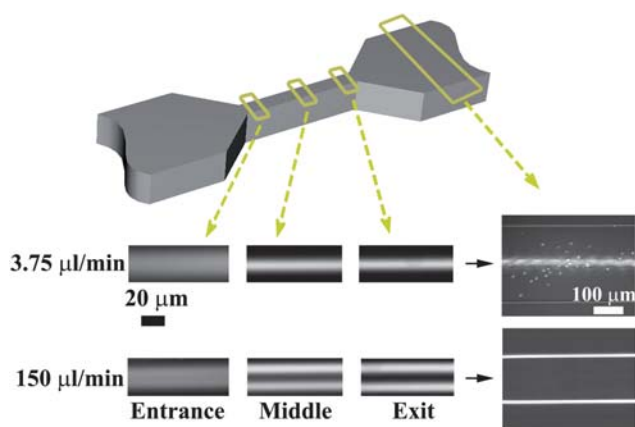


Fig. 2 Particle migration in a flow-through electroporation device with a straight electroporation section. The device has the same dimensions as the spiral arrangement in Fig. 1 except that the narrow section is straight. Overlay fluorescence images show SYTO 16 stained CHO cells flowing in the device at flow rates of 3.75 and 150 $\mu\text{l}/\text{min}$.

symmetrically positioned about the centerline (Fig. 2), also consistent with previous observations.^{14,15} These equilibrium focusing positions move further outward toward the vertical channel walls as the flow rate increases (Fig. 2).

We next investigated flow-through electroporation of CHO cells using both straight and spiral shaped channels. In both cases, the wide sections are a factor of 14.3 larger than the narrow

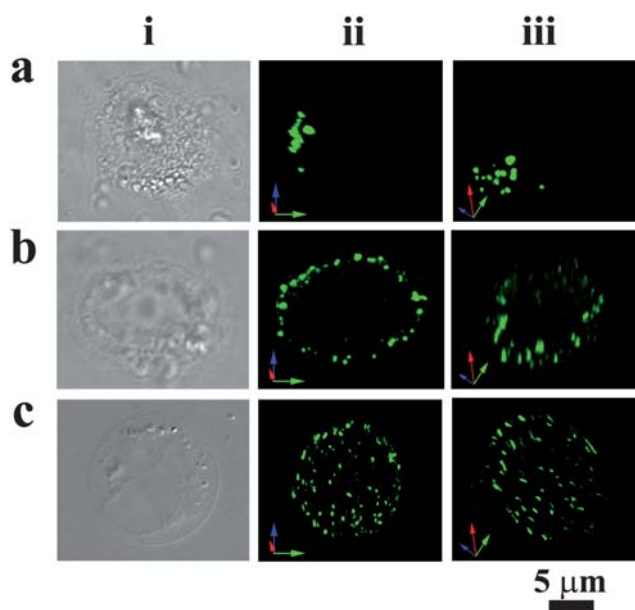


Fig. 3 Phase contrast (i) and 3D reconstruction images generated by confocal fluorescence imaging (ii and iii are from different angles) of CHO cells processed by flow-through electroporation devices under different conditions. The cells are delivered with YOYO-1 labeled plasmid DNA. (a) Cells processed by flow-through electroporation in a straight microchannel (field intensity 900 V/cm, duration 0.5 ms). (b) Cells processed by flow-through electroporation in a straight microchannel (flow rate 150 $\mu\text{l}/\text{min}$, field intensity 700 V/cm, duration 5 ms). (c) Cells processed by flow-through electroporation in a spiral microchannel (flow rate 150 $\mu\text{l}/\text{min}$, field intensity 700 V/cm, duration 5 ms). The videos of these 3D reconstruction images are available in the **ESI Movies 1–3**.†

section, rendering the electric field intensity higher by the same factor in the narrow section than that in the wide sections when a constant voltage is applied across the channel (with two platinum electrodes in the inlet and outlet reservoirs).¹ When a mixture of cells and plasmid DNA is pumped through the microchannel network, the cells are exclusively electroporated in the narrow section because the field intensity in the wide sections (28–56 V/cm) is substantially lower than the electroporation threshold for most mammalian cells (>300–400 V/cm). We observed the delivery of exogenous DNA molecules (fluorescently labeled with YOYO-1) into the CHO cells using confocal fluorescence microscopy. Because the DNA molecules can only penetrate the cell membrane within the electroporated zone, and since they are uniformly distributed throughout the microchannel, the fluorescence on or inside the cell membrane essentially “maps” the area that has been electroporated to the extent that allows DNA entry. In a straight microchannel with an electroporation duration of 0.5 ms (*i.e.*, the time for cells to travel through the narrow electroporation section), DNA delivery is confined to a narrow zone in the vicinity of one pole of the cell (Fig. 3a). This result is in agreement with comparable results obtained in static electroporation systems,^{8,9} and is consistent with a unidirectional flow profile through the electroporation section without cell rotation. Longer electroporation durations (5 ms) in the straight microchannel produce DNA delivery within a thin circular strip around the cell equator due to the onset of rotation about a fixed axis (Fig. 3b). When identical flow conditions and electric field parameters are applied in a spiral microchannel of the same dimensions, however, the confocal images appear dramatically different with DNA delivery uniformly distributed over the entire cell surface as a consequence of the combined effects of rotation and transverse advection during electroporation (Fig. 3c). **ESI Fig. S2**† shows the epi-fluorescence images of the larger cell populations which indicate that the images in Fig. 3 are representative of the cell populations.

The enhanced DNA uptake based on flow-through electroporation in curvilinear channels has important implications. In Fig. 4a, we show the transfection of CHO cells by pEGFP-C1 vector using both straight and spiral shaped microchannels of the same dimensions. Under the same flow rate and electric field conditions, the transfection efficiency in the spiral geometry is about two-fold higher than that achieved in the straight channel devices. Cell viability after electroporation is similar in both microchannel geometries (Fig. 4b). The cell viability was not compromised by electroporation significantly due to the fairly short field duration and medium field intensity. The shear stress that cells experience here is not excessive compared to in other established cell-handling techniques such as flow cytometry. The similar viability in the straight and spiral channels suggests that the cell viability is independent of the membrane area that is permeabilized. Instead, the cell viability is possibly much more affected by Joule heating which is determined only by the field intensity/duration and identical in the two devices.

Discussion

In order to better understand how these hydrodynamic effects act to produce enhanced transfection efficiency, we consider the

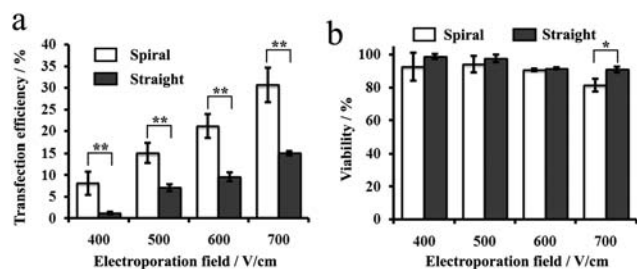


Fig. 4 The delivery and expression of a plasmid DNA vector (pEGFP-C1) in CHO cells by flow-through electroploration devices with different geometries. In both the spiral (white bars) and straight (dark bars) electroploration devices, the electroploration field intensity is varied from 500 to 800 V/cm (flow rate 150 μ l/min, duration 5 ms). All data points are generated by experiments in triplicate and \sim 5,000 cells are examined in each trial. Two-tailed student's t test was applied to evaluate the data. (*) indicates significant difference at $P < 0.05$ and (**) indicates significant difference at $P < 0.01$. (a) Transfection efficiency of cells (the number of cell expressing EGFP divided by the number of living cells) examined two days after electroploration. (b) The viability of the cells (the number of living cells divided by the total cell number) examined two days after electroploration.

physics of microscale particle migration in curvilinear channels.^{13,16–20} Suspended particles are subjected to the laminar flow field inside a curved microfluidic channel and experience a combination of inertial lift and drag forces due to the transverse Dean flow. When the magnitude of these forces is similar, the convected particles migrate to occupy lift-induced equilibrium positions that minimize the Dean flow effects. On the other hand, when the drag is substantially larger than the lift force, the particles become displaced from these equilibrium positions and begin to follow the Dean vortex pattern.^{19,20} In comparison, particles that flow in a straight channel are focused into multiple equilibrium positions due to inertial self-ordering.^{13,21} The strong dependence of these effects on particle size has led to interest in harnessing Dean flow effects for particle sorting and separation applications.^{13,19,20,22} However, these effects have not been explored in connection with manipulation of particle orientation or DNA delivery into cells. There are two important Reynolds numbers that characterize the flow of particles in a channel.^{13,23} The channel Reynolds number (R_c) and the particle Reynolds number (R_p) are defined by:

$$R_p = \frac{U_m a^2}{\nu D_h} = \frac{U_m D_h}{\nu} \cdot \frac{a^2}{D_h^2} = R_c \left(\frac{a}{D_h} \right)^2$$

where U_m is the maximum velocity in the cross section, and a is the diameter of the particle, ν is kinematic viscosity and D_h is the hydraulic diameter which is defined as $2wh/(w+h)$ (with w and h being the width and depth of the channel). The Dean number De is used to characterize the curvature effects in a curvilinear channel and is defined as: $De = \frac{\bar{U} D_h}{\nu} \left(\frac{D_h}{2R} \right)^{\frac{1}{2}} = Re \left(\frac{D_h}{2R} \right)^{\frac{1}{2}}$, where R is the radius of curvature of the channel, \bar{U} is the mean axial velocity, and Re is the Reynolds number ($Re = \frac{\bar{U} D_h}{\nu}$). In our experiments with spiral-shaped channels, we observe that the particles are entrained in Dean vortices when $R_c = 50$ – 100 and the average $De = 13$ – 26 . The dimensionless inertial force ratio R_f (with $R_f \sim$

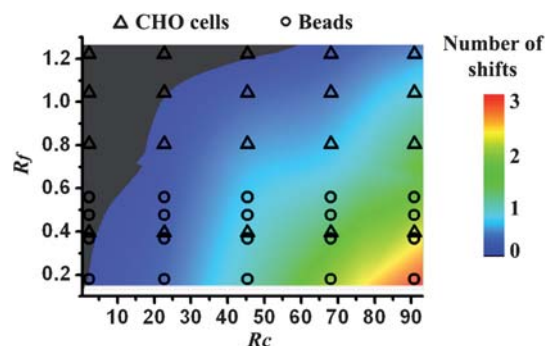


Fig. 5 State diagram depicting how the extent of entrainment in the secondary flow (quantified in terms of the number of shifts across the channel centerline made by the particle streams) depends on the inertial force ratio R_f and channel Reynolds number R_c . Strongest entrainment occurs under a combination of low R_f and high R_c (the lower right corner in the graph), suggesting that this regime provides optimal conditions for vortex-assisted electroploration. The number of centerline shifts at a particular R_f was determined by dividing the spiral section into 4 segments of equal length with average radii of curvature R of 100.5, 205, 265.5, and 311 μ m. The number of shifts by CHO cells ($a \sim 14.6 \mu$ m, triangle) and polystyrene beads ($a \sim 9.9 \mu$ m, circle) within these segments is indicated by the color scale of the contour plot.

$F_L/F_D = 2Ra^2/D_h^3$) expressing the relative magnitudes of inertial lift forces (F_L) and drag forces due to the secondary flow (F_D) has recently been proposed as a useful parameter to identify conditions favorable for particle entrainment in the secondary flow.²⁴ In our experiments, we take the number of lateral shifts (across the channel centerline) made by the particle (bead or cell) stream along a fixed channel length as a measure of entrainment. Plotting these centerline crossings against R_f and R_c enables the key flow and geometric effects to be collapsed onto a state diagram, providing a valuable design tool (Fig. 5). This analysis suggests that a combination of low R_f and high R_c provides the most favorable conditions for vortex-assisted electroploration by inducing a high degree of entrainment in the secondary flow. In general, we observe that particle displacements across the centerline occur more frequently per unit contour length of the channel when they are close to the center of the spiral (Fig. 1). This is characteristic of the transverse migration along a Dean vortex. The velocity in the rotational flow due to the Dean drag U_d scales as $U_d \sim De^2 \nu / D_h$ with ν being the kinematic viscosity.¹³ Assuming the particle will cover a circular path L_d in the transverse direction with a length of $\frac{3}{2} D_h$,²⁵ the channel length L_c covered during the period that the particle travels through a complete circular path along a Dean vortex will therefore be $L_c = \bar{U} \frac{L_d}{U_d} \sim \frac{3\bar{U} D_h^2}{2\nu De^2}$. The equation shows that L_c becomes short (*i.e.*, more frequent centerline crossings) close to the spiral center and at high De , consistent with our observations.

Based on the pattern of DNA delivery shown in Fig. 3, we can now infer the nature of the cell migration phenomena occurring in different microchannel geometries during flow-through electroploration. When flow-through electroploration occurs in a curved microchannel, the DNA delivery over the entire cell surface is a result of the induced cell motion in the spiral channel segment, which involves a combination of rotation and

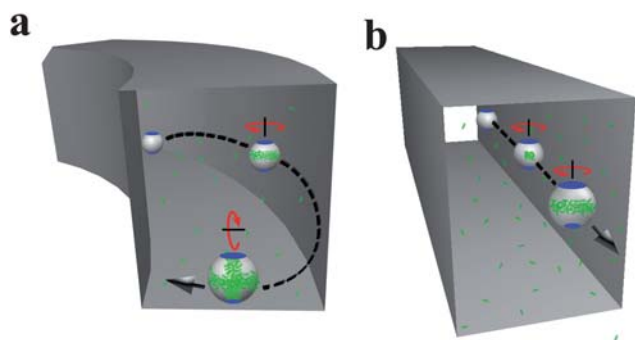


Fig. 6 Vortex-assisted electroporation. (a) In a curved microchannel, the resulting hydrodynamic effects subject a cell to a combination of transverse vortex motion and rotation that enables the entire membrane surface to be uniformly permeabilized. These effects are illustrated at two specific locations. The rotation at the first position induces electroporation/DNA delivery around the equator, whereas a different region is permeabilized due to the rotation occurring at the second position that is downstream along the path of the vortex. (b) In contrast, only a small fraction of the membrane is permeabilized in a straight microchannel under the same flow conditions without the transverse motion.

transverse advection following the Dean vortex pattern. Fig. 6a illustrates how this process would allow cells to experience electroporation over their entire surface. When a cell simultaneously experiences rotation due to the near-wall shear field coupled with transverse motion due to the Dean vortex flow, different parts of the cell surface are continuously exposed to a sufficiently high transmembrane potential to permit electroporation. In comparison, in a straight channel cells experience rotation about an axis that is parallel to the vertical walls as they travel through the electroporation section (Fig. 6b). These effects begin to influence electroporation when the electric pulse duration is long enough (e.g. ~ 5 ms) by expanding the zone of DNA delivery from the pole to a circular strip. Previous literature indicates that such free rotation of particles occurs in response to imposed shear in a Poiseuille flow,²⁶ and that the cell-wall friction due to hydrodynamic interactions can also affect the rotation rate.²⁷ The rotation rate is estimated to be ~ 830 revolutions/s at the flow rate of $150 \mu\text{L}/\text{min}$ in our device, based on experimental results in the literature.²⁸ This is consistent with the fact that an electroporation duration of 5 ms in the straight channel generates a circular DNA delivery zone while 0.5 ms duration constrains the delivery to a much smaller area, as shown in Fig. 3. Finally, it needs to be noted that entrainment in the secondary Dean flow may not be entirely necessary. It is possible that similar effect is achievable by imposing conditions whereby the cells become inertially focused at prescribed equilibrium positions but are still exposed to torque generated by the secondary flow, thereby inducing different rotation characteristics than those due to shear field.

While curvature-induced inertial flows have been widely studied in single-phase fluids, these phenomena are only beginning to be fully understood and appreciated in particle laden suspensions.²⁹ With proper design, these effects can be harnessed

to greatly enhance gene delivery efficiency with only a simple modification to the design of existing continuous flow electroporation systems. This method is inherently robust and readily amenable to both scaling up and down³⁰ for processing cell samples spanning a wide range of volumes, including small volume samples from scarce sources.

Acknowledgements

The authors acknowledge support from NSF CBET-0747105, Wallace H. Coulter Foundation, ARS-USDA (through CFSE at Purdue University), and USDA-NRI 2009-35603-05059.

References

- H. Y. Wang and C. Lu, *Anal. Chem.*, 2006, **78**, 5158–5164.
- Y. Huang and B. Rubinsky, *Sens. Actuators, A*, 2003, **104**, 205–212.
- H. Lu, M. A. Schmidt and K. F. Jensen, *Lab Chip*, 2005, **5**, 23–29.
- Z. Fei, S. Wang, Y. Xie, B. E. Henslee, C. G. Koh and L. J. Lee, *Anal. Chem.*, 2007, **79**, 5719–5722.
- A. Valero, J. N. Post, J. W. van Nieuwkastele, P. M. ter Braak, W. Kruijer and A. van den Berg, *Lab Chip*, 2008, **8**, 62–67.
- A. M. Skelley, O. Kirak, H. Suh, R. Jaenisch and J. Voldman, *Nat. Methods*, 2009, **6**, 147–152.
- J. C. Weaver and Y. A. Chizmadzhev, *Bioelectrochem. Bioenerg.*, 1996, **41**, 135–160.
- E. Tekle, R. D. Astumian and P. B. Chock, *Proc. Natl. Acad. Sci. U. S. A.*, 1994, **91**, 11512–11516.
- M. Golzio, U. S. A., 2007, **104**, 18892–18897.
- M. Rebersek, C. Faurie, M. Kanduser, S. Corovic, J. Teissie, M. P. Rols and D. Miklavcic, *BioMed. Eng. Online*, 2007, **6**, 25.
- J. Wang, N. Bao, L. L. Paris, H. Y. Wang, R. L. Geahlen and C. Lu, *Anal. Chem.*, 2008, **80**, 1087–1093.
- H. Y. Wang and C. Lu, *Biotechnol. Bioeng.*, 2008, **100**, 579–586.
- D. Di Carlo, D. Irimia, R. G. Tompkins and M. Toner, *Proc. Natl. Acad. Sci. U. S. A.*, 2007, **104**, 18892–18897.
- M. Abkarian, M. Faivre, R. Horton, K. Smistrup, C. A. Best-Popescu and H. A. Stone, *Biomed. Mater.*, 2008, **3**, 034011.
- A. Bhagat, S. Kuntaegowdanahalli and I. Papautsky, *Phys. Fluids*, 2008, **20**, 101702.
- W. R. Dean, *Philos. Mag.*, 1927, **4**, 208–223.
- W. R. Dean, *Philos. Mag.*, 1928, **5**, 673–695.
- A. P. Sudarsan and V. M. Ugaz, *Proc. Natl. Acad. Sci. U. S. A.*, 2006, **103**, 7228–7233.
- J. Seo, M. H. Lean and A. Kole, *Appl. Phys. Lett.*, 2007, **91**, 033901.
- A. A. S. Bhagat, S. S. Kuntaegowdanahalli and I. Papautsky, *Lab Chip*, 2008, **8**, 1906–1914.
- J. F. Edd, D. Di Carlo, K. J. Humphry, S. Koster, D. Irimia, D. A. Weitz and M. Toner, *Lab Chip*, 2008, **8**, 1262–1264.
- D. Di Carlo, J. F. Edd, D. Irimia, R. G. Tompkins and M. Toner, *Anal. Chem.*, 2008, **80**, 2204–2211.
- E. S. Asmolov, *J. Fluid Mech.*, 1999, **381**, 63–87.
- D. R. Gossett and D. Di Carlo, *Anal. Chem.*, 2009, **81**, 8459–8465.
- S. Ookawara, R. Higashi, D. Street and K. Ogawa, *Chem. Eng. J.*, 2004, **101**, 171–178.
- L. Y. Zeng, S. Balachandar and P. Fischer, *J. Fluid Mech.*, 2005, **536**, 1–25.
- M. E. Staben, A. Z. Zinchenko and R. H. Davis, *Phys. Fluids*, 2003, **15**, 1711–1733.
- D. Di Carlo, J. F. Edd, K. J. Humphry, H. A. Stone and M. Toner, *Phys. Rev. Lett.*, 2009, **102**, 094503.
- D. Di Carlo, *Lab Chip*, 2009, **9**, 3038–3046.
- T. Geng, Y. Zhan, H. Y. Wang, S. R. Witting, K. G. Cornetta and C. Lu, *J. Controlled Release*, 2010, **144**, 91–100.